IEC Report

Sean Wu
July 29, 2019

Abstract

In this paper, the indirect evaporative cooler (IEC) is explored as an energy-efficient and environmentally-friendly alternative to conventional air conditioning systems. A 1D simulation model was first developed and validated against two sets of experimental data from existing literature. Furthermore, various design parameters and input conditions were analyzed along with several configurations to find the optimal design. Using the simulation model, it was found that the channel length could be reduced by up to 50% to a length of 1 to 1.5 metres. This can be achieved by adding a dehumidifier or a conventional air conditioning system to manipulate inlet humidity or output air flow temperatures.

Introduction

Given Singapore's proximity to the equator, it has a tropical climate with high temperatures and humid conditions throughout the year. According to data collected by the Changi Climate Station between 1981 and 2010, the mean daily maximum temperature is around 32 °C, while the relative humidity ranges from 70% to 90% during the day [1]. These extremely hot conditions can cause several serious heat-related illnesses, like heat stroke, which is a major concern for vulnerable demographics like the young and the eldery [2].

Currently, most Singaporean homes and buildings use conventional vapor compression air conditioning systems. These systems compress and expand a fluid in order to remove heat from the system and reduce temperatures. However, sustaining the high pressures required to remove heat is very energy intensive. Furthermore, these systems also use harmful refrigerants like chlorofluorocarbons and hydrochlorofluorocarbons, which harm the ozone layer in the atmosphere and contribute to global warming [3]. In tropical climates, the use of air conditioning can represent over 50% of energy expenditure in buildings [4]. Thus, improvements over current air conditioning methods can greatly reduce energy use, costs, and environmental impact.

Another method of air conditioning is evaporative cooling. This method capitalizes on the high latent heat of vaporization of water by passing air flow above thin films of water. As the water evaporates, heat is drawn from the air to fuel the process of vaporization, causing the overall air flow temperature to decrease. Since the principal cooling mechanism is evaporation, this method is heavily dependent on the inlet air humidity and its cooling potential is restricted by the wet bulb temperature of the ambient air [5]. The tradeoff, however, is a significantly reduced energy cost over conventional air conditioning units since evaporative cooling systems have a higher energy efficiency (COP) [6].

Evaporative cooling can be further subdivided into direct evaporative cooling (DEC) and indirect evaporative cooling (IEC). As shown in Fig. 1a, DECs consist of a single air channel that contains both the water film and the product air flow being delivered. Consequently, the evaporated water is added to the product air flow, increasing the moisture content and relative humidity. In arid climates, the added humidity is less noticeable, but the increased moisture can be a serious issue in more humid climates like Singapore. The added humidity can cause discomfort and can also lead to hygienic issues if the system is poorly maintained [7]. In contrast, IECs (shown in Fig. 1b) separate the air flow into separate channels. The working air flow is passed through the wet channel containing the water film, while the product air is passed through an adjacent dry channel. The temperature gradient between the wet and dry channels causes heat to be transferred from the hotter dry channel, through the boundary plate by conduction, and into the water film of the wet channel. Heat can then be transferred to the working air flow by sensible and latent heat transfer. In this way, no moisture is added to the product air before being delivered, making IECs more suitable in Singapore. Thus, the rest of this paper will focus on indirect evaporative coolers since the lack of added moisture is important for use in the Singaporean climate.

a.

b.

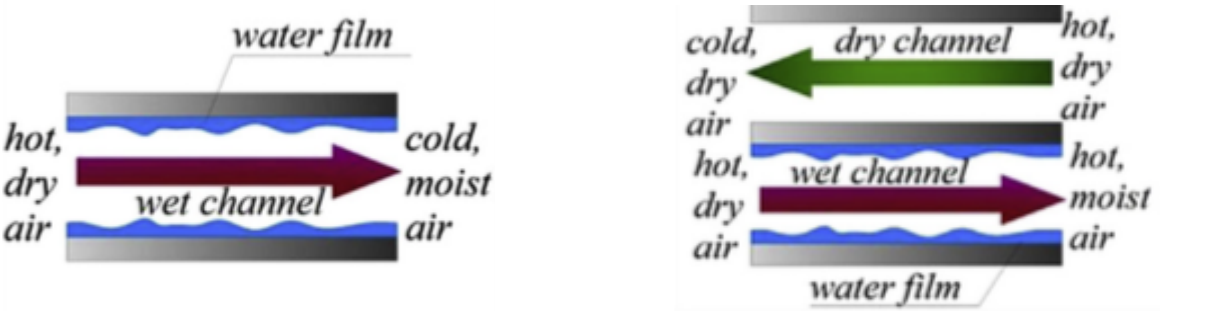

Figure 1. Diagrams depicting the channels of different types of evaporative coolers. (a) Direct Evaporative Cooling. (b) Indirect Evaporative Cooling. [8]

Nomenclature

c_{pa} Specific heat capacity of dry air [J/kg K]
c_{pm} Specific heat capacity of moist air [J/kg K]
c_{pw} Specific heat capacity of water vapour [J/kg K]
c_{pda} Specific heat capacity of moist air in dry channel [J/kg K]
c_{pwa} Specific heat capacity of moist air in wet channel [J/kg K]
D Hydraulic diameter [m]
dA Differential plate area contained in control volume [m^2]
$d\dot{Q}_d$ Rate of sensible heat transfer in dry channel [W]
$d\dot{Q}_{wL}$ Rate of latent heat transfer in wet channel [W]
$d\dot{Q}_{ws}$ Rate of sensible heat transfer in wet channel [W]
dT_{dry} Differential temperature change in dry channel [°C]
dT_{wet} Differential temperature change in wet channel [°C]
$d\omega$ Differential absolute humidity ratio change [kg/kg]
H Channel height [m]
h Heat transfer coefficient [W/m^2K]
h_{fg} Latent heat of evaporation [J/kg]
h_m Mass transfer coefficient [kg/m^2s]
k Thermal conductivity of air [W/m K]
k_p Thermal conductivity of plate [W/m K]
L Channel length [m]
Le Lewis Number
$\dot{m_{ad}}$ Mass flow rate in dry channel [kg/s]
$\dot{m_{aw}}$ Mass flow rate in wet channel [kg/s]
$\dot{m_v}$ Water vapour evaporation rate in wet channel [kg/s]
Nu Nusselt Number
P_{ws} Saturation pressure over water film [Pa]
T_{air} Air temperature [°C]
T_{dry} Temperature of dry channel air flow [°C]
T_{wet} Temperature of wet channel air flow [°C]
T_{wa} Temperature of water film [°C]
τ Plate thickness [m]
U Combined heat transfer coefficient [W/m^2K]
W Channel width [m]
ω_{air} Absolute humidity ratio over water film [kg/kg]
ω_s Absolute humidity ratio in wet channel air flow [kg/kg]

Literature Review

Indirect evaporative coolers can be further subdivided into parallel flow, cross-flow, and counter-flow (regenerative) configurations as seen in Fig. 2a-c. However, this paper will focus specifically on the counter-flow configuration combined with the Maisotsenko cycle (M-Cycle).

The Maisotsenko cycle couples heat transfer with evaporation such that the IECs can overcome the ambient wet bulb temperature limit and approach the theoretical ambient dew point temperature limit for the outlet product temperature [9]. For the M-Cycle, the working air is precooled before being used to draw heat from the product air. This allows for a larger temperature gradient and more effective heat transport, allowing the output temperature to drop below the wet bulb temperature approach the theoretical ambient dew point temperature limit [7]. In practice, this is done by stacking the wet channel on top of the dry channel and diverting a fraction of the product air into the wet channel to be used as the working air. However, this results in less product air being delivered as output, so many wet and dry channels are typically used along with a larger input air flow.

In existing scientific literature, the topic of IECs has been developed both through experimental results and new theoretical models. Pandelis et al. used an ε-NTU model to mathematically represent an IEC under temperate climate conditions. Through their research, they found that IECs can operate efficiently under a wide range of air flow conditions, making them suitable for use in air conditioning [10]. Furthermore, Ren and Yang developed an analytical approach, that through comparison, were found to strongly verify existing numerical simulations [11]. In their analytical model, Ren and Yang also considered nonunity Lewis values, incomplete surface wetting, and various other factors. Another analytical model was also developed by Cui et al by using a modified LMTD method. Their model had a maximum deviation of 8% from experimental results and could be computed very quickly [12]. In another study, Pandelis et al. compared

counter- and cross-flow configurations while considering water vapour condensation. They found that the counter-flow model had greater sensible and latent cooling potential than the cross-flow configuration, but achieved a lower Energy Efficiency Ratio and required higher investment costs [13]. Finally, Riangvilaikul and Kumar performed an experimental study and found that the inlet velocity should be kept under 2.5 m/s for inlet temperatures greater than 30 ^{o}C [7]. They also showed through experiments that IECs performed well under various conditions in dry, moderate, and humid climates.

a.

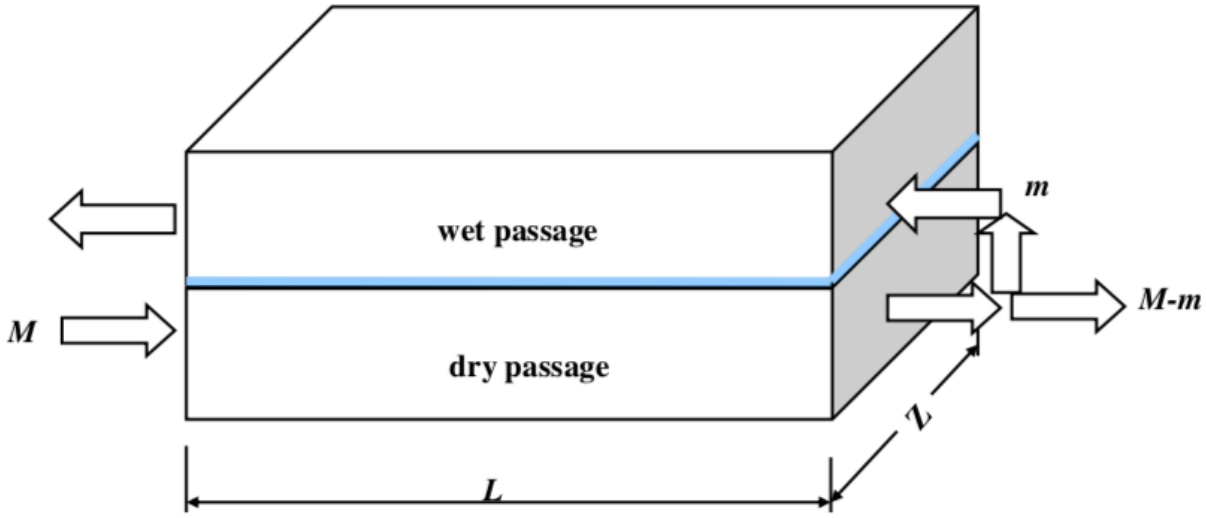

Figure 2. Comparison of different indirect evaporative cooling configurations. (a) Diagram of counter-flow (Regenerative) configuration [14]. (b) Diagram of cross-flow configuration [13]. (c) Diagram of parallel flow configuration [15].

Mathematical Model and Simulation Method

The counter-flow M-Cycle Indirect Evaporative Cooler (IEC) was simulated by splitting the IEC into many control volumes along its length in the x-direction. Given the thin height of each control volume, the air temperatures in each channel were assumed to be constant and thus temperature remained fixed in the y-direction. Finally, the temperatures were also assumed to be constant along the channels' width in the z-direction. This meant that the IEC only needed to be simulated in the x-direction, which greatly simplified calculations. A sample control volume showing the sensible and latent heat transfer involved is shown in Fig. 3.

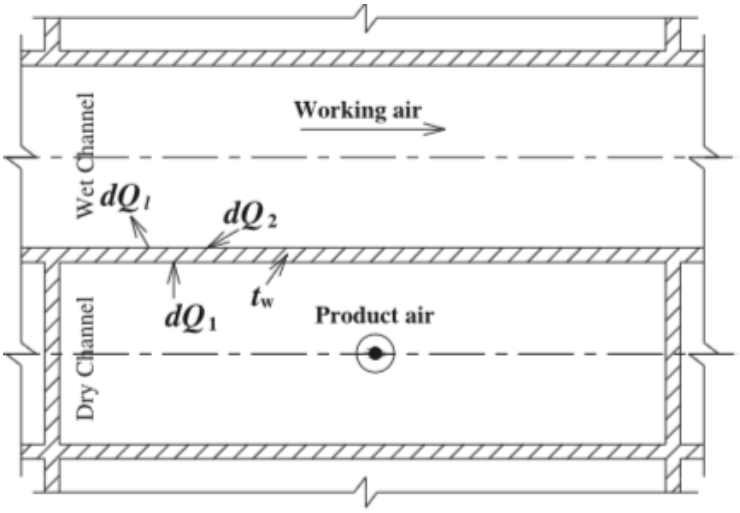

Figure 3. Diagram of control volume showing sensible heat transfer in the dry channel as well as sensible and latent heat transfer in the wet channel [16].

Summary of key assumptions:

1. Lewis Number is unity (Le = 1)
2. Fully developed air flow [17]
3. Air flow consists of an ideal, incompressible gas mixture of dry air and moisture [10]
4. Longitudinal mass transfer of water molecules and longitudinal heat transfer along the walls and in the fluid are negligible [10]
5. Nusselt numbers and heat transfer coefficients are constant
6. Air temperatures along the y- and z-axes in each control volume are constant
7. Heat transfer to the external environment is negligible [17]
8. The air above the water film is fully saturated and there is a uniform distribution of water vapour along the wet channel [6]

To calculate heat transfer coefficients for both wet and dry channels, the Nusselt number was first found. Assuming a fully developed air flow and a rectangular channel, the Nusselt Number is constant value [18]:

$$Nu = 4.12 \quad (1)$$

The hydraulic diameter must also be calculated for each channel:

$$D = \frac{2WH}{W+H} \quad (2)$$

Finally, the heat transfer can be calculated for both channels using the Nusselt number relation. Changes in the thermal conductivity of air along the channel were assumed to be negligible, allowing the heat transfer coefficient to be treated as constant.

$$h = \frac{Nu\ k}{D} \quad (3)$$

The mass flow rates in each channel are related by the working air ratio:

$$Working\ Air\ Ratio = \frac{\dot{m}_{aw}}{\dot{m}_{ad}} \quad (4)$$

The specific heat capacity was calculated at each control volume by first calculating the specific heat capacity of dry air at that temperature using equation 5 and then factoring in the effects of moisture in equation 6 [19]. A value of c_{pw} = 1.86x10^{-3} J/kg K was used for the specific heat capacity of H_2O vapour.

$$c_{pa}(T_{air}) = 1.0038 \cdot 10^3 + 3 \cdot 10^{-2} T_{air} + 4 \cdot 10^{-4} {T_{air}}^2 \quad (5)$$

$$c_{pm} = c_{pa}(T_{air}) + \omega_{air} c_{pw} \quad (6)$$

Dry Channel

The temperature difference between the dry and wet channels leads to convection in the z-direction of the dry channel followed by conduction through the plate boundary. Thus, a combined heat transfer coefficient was used to include both methods of heat transfer.

$$U = \frac{1}{\frac{1}{h} + \frac{\tau}{k_p}} \quad (7)$$

The rate of sensible heat transferred can then be calculated using equation 8. This rate and the specific heat capacity calculated using equation 5 then gives the differential temperature change between each control volume.

$$d\dot{Q}_d\,(i) = U(\,T_{dry}(i) - T_{wa}(i))\,dA \quad (8)$$

$$dT_{dry}(i) = \frac{dQ\,(i)}{\dot{m}_{ad}\,c_{pda}\,(i)} \quad (9)$$

Wet Channel

Similarly to equation 8 and 9 for the dry channel, the equations 10 and 11 give the rate of sensible heat transferred and the differential temperature change, respectively.

$$dQ_{ws}(i) = h\,(\,T_{wa}\,(i) - T_{wet}\,(i)\,)\,dA \quad (10)$$

$$dT_{wet}(i) = \frac{d\dot{Q}_{ws}(i)}{\dot{m}_{aw}\,c_{pwa}(i)} \quad (11)$$

However, the wet channel also has latent heat transfer due to evaporation in the water film. This evaporation is caused by the water concentration difference in the water film and the air flow in the wet channel. This concentration difference can be approximated by calculating the difference in absolute humidity in the saturated air just above the water film surface and the surrounding air. To find the humidity difference, the saturation pressure must first be calculated with equation 12.

$$\ln\left(P_{ws}(i)\right) = \frac{a_1}{T_{wa}} + a_2 + a_3\, T_{wa}\ (i) + a_4 {T_{wa}}^2(i) + a_5 {T_{wa}}^3(i) + a_6 ln(T_{wa}(i)) \quad (12)$$

$$a_1 = -5.80002206 \cdot 10^3$$
$$a_2 = 1.39149933 \cdot 10^0$$
$$a_3 = -4.8640239 \cdot 10^{-2}$$
$$a_4 = 4.1764768 \cdot 10^{-5}$$
$$a_5 = -1.4452093 \cdot 10^{-8}$$
$$a_6 = 6.5459673 \cdot 10^0$$

where 0 °C < T_{wa} < 200 °C

The absolute humidity ratio over the water film surface can be calculated using the saturation pressure in equation 13.

$$\omega_s(i) = 0.621945\ \frac{P_{ws}(i)}{P_{atm} - P_{ws}\,(i)} \quad (13)$$

Using the Lewis analogy and assuming that Le = 1, the mass transfer coefficient can be calculated accordingly [18].

$$h_m(i) = \frac{h}{c_{pa(i)}\, Le} \approx \frac{h}{c_{pa(i)}} \quad (14)$$

This then allows the H_2O evaporation rate to be calculated.

$$\dot{m}_v = h_m(\,\omega_s(i) - \omega_{air}(i)\,)dA \quad (15)$$

Furthermore, the latent heat of evaporation can also be calculated:

$$h_{fg}(i) = b_1 {T_{wa}}^2(i) + b_2 T_{wa}(i) + b_3 \quad (16)$$

$$b_1 = 6.15397082 \cdot 10^{-1}$$
$$b_2 = -2.342205094962 \cdot 10^3$$
$$b_3 = 2.50065738532596 \cdot 10^6$$

where 10 °C < T_{wa} < 50 °C

Combining the evaporation rate and the latent heat of evaporation from equation 16, the rate of latent heat transferred can be finally calculated using equation 17.

$$d\dot{Q}_{wL}(i) = h_{fg}\dot{m}_v \quad (17)$$

Using the mass flow rate of air and the wet channel and the rate of evaporation, the differential change in absolute humidity can then be calculated using equation 18.

$$d\omega_{air}\ (i)\ =\ \frac{\dot{m}_{av(i)}}{\dot{m}_{aw}} \tag{18}$$

Finally, if the heat transfer rates are balanced within a small margin of error, ε, the temperatures and air humidity ratio can be updated for the next control volume using equations 19-21:

If $d\dot{Q}_d\ (i)\ -\ (dQ_{ws}(i) + \ d\dot{Q}_{wL}(i))\ <\ \epsilon$:

$$T_{dry}(i+1)\ =\ T_{dry}(i)\ +\ dT_{dry}(i) \tag{19}$$
$$T_{wet}(i+1)\ =\ T_{wet}(i)\ +\ dT_{wet}(i) \tag{20}$$
$$\omega_{air}(i+1)\ =\ \omega_{air}(i)\ + d\omega_{air}(i) \tag{21}$$

Solution of Governing Equations

The mathematical model explained above can be simulated in MATLAB using 3 nested loops. The outermost loop is for guessing the outlet temperature while the second outermost loop is for iterating over all the control volumes along the IEC's length. Finally, the innermost loop is used to guess the water temperature of the specific control volume such that the heat transfer rates are properly balanced.

During the simulation, a primary outlet temperature is assumed and the simulation works backward from the primary outlet to the inlet. The program analyzes the air temperatures for each control volume and finds the water temperature that results in the dry channel sensible heat flow balancing with the sum of sensible and latent heat transfer in the wet channel. This allows the differential temperature and humidity changes to be calculated and the temperature condition of the next control volume can be found. The simulation then continues until it reaches the final control volume at the primary inlet air. If the final primary air temperature matches the actual inlet air temperature, then the original outlet temperature assumption is correct since the balancing of heat flow must be satisfied over the entire length. If the values do not match, then a new outlet temperature is assumed. The specific details of the simulation process can be found in the simulation flow chart in Fig. 4.

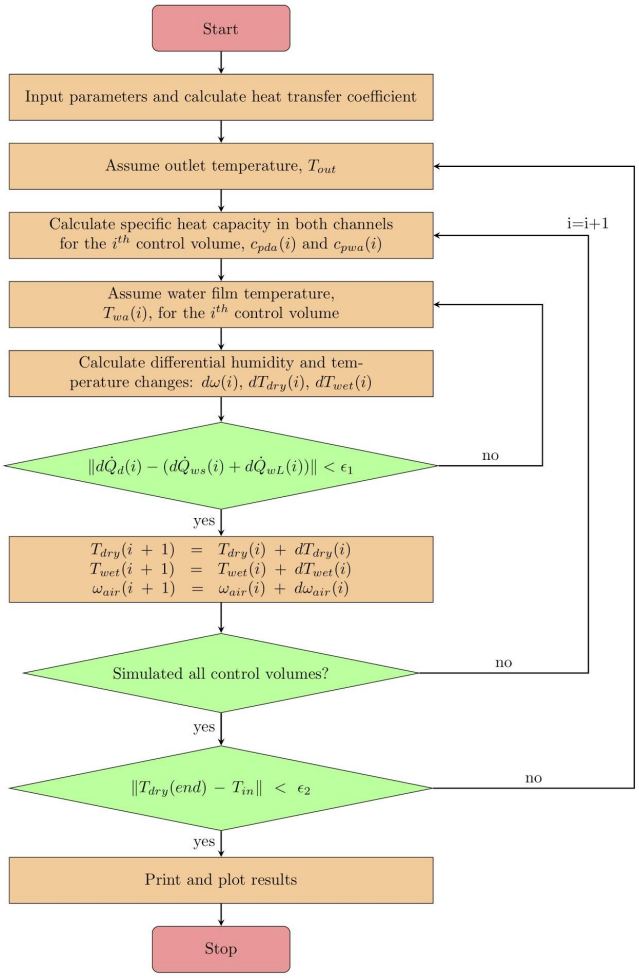

Figure 4. Flow chart for a 1D simulation of an Indirect Evaporative Cooler

Validation

To validate the results, the mathematical model was compared with the two trials of experimental results performed by Jie Lin et al. In each trial, the two closest fitting methods were using Nu = 4.861 as suggested by Hasan and using Nu = 4.12 as proposed by Anisimov [14,18]. As evident from the graphs in Fig 5a-d and Table 2, the mathematical model using Nu = 4.12 as suggested by Anisimov most closely matches the experimental data. While using Nu = 4.12 had a greater maximum error in both validation trials, the issue is localized to the outlet of the primary air. As shown by the consistent average error and the graphs, Nu = 4.12 performs better in general and was thus used in the mathematical model.

	Jie Lin Dataset A	Jie Lin Dataset B
Inlet Temperature [°C]	32.6	38.2
Inlet Absolute Humidity [g/kg]	14.0	10.2
Inlet Velocity [m/s]	2.1	2.0
Working Air Ratio	0.32	0.31

Table 1. Input conditions for the 2 experimental datasets from Jie Lin et al. [20]

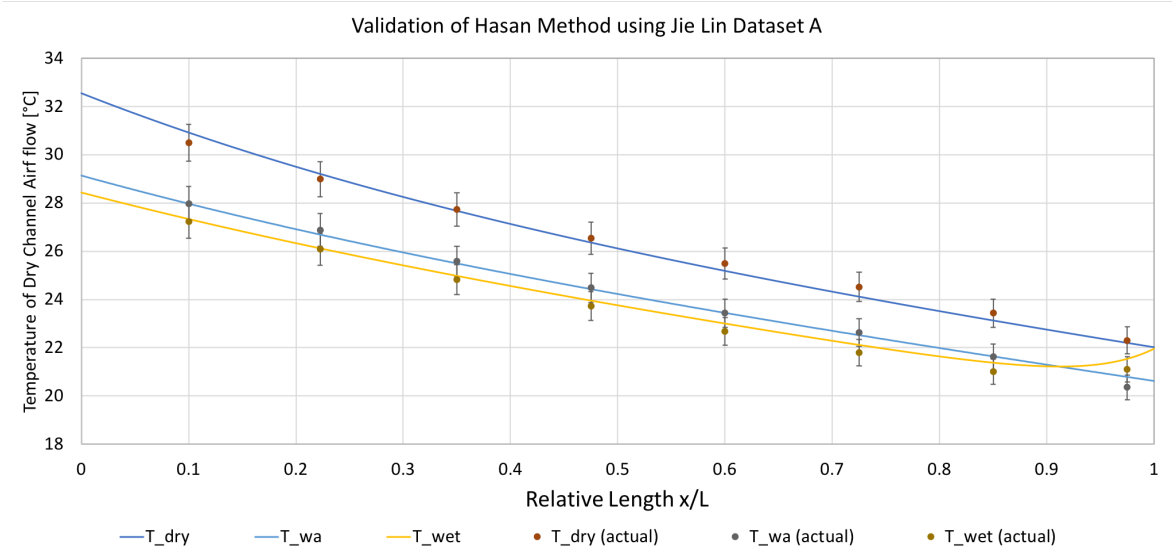

Figure 5a. Simulation for Jie Lin et al.'s dataset A using Hasan's method (Nu = 4.861). Error bars indicate the range for 2.5% error.

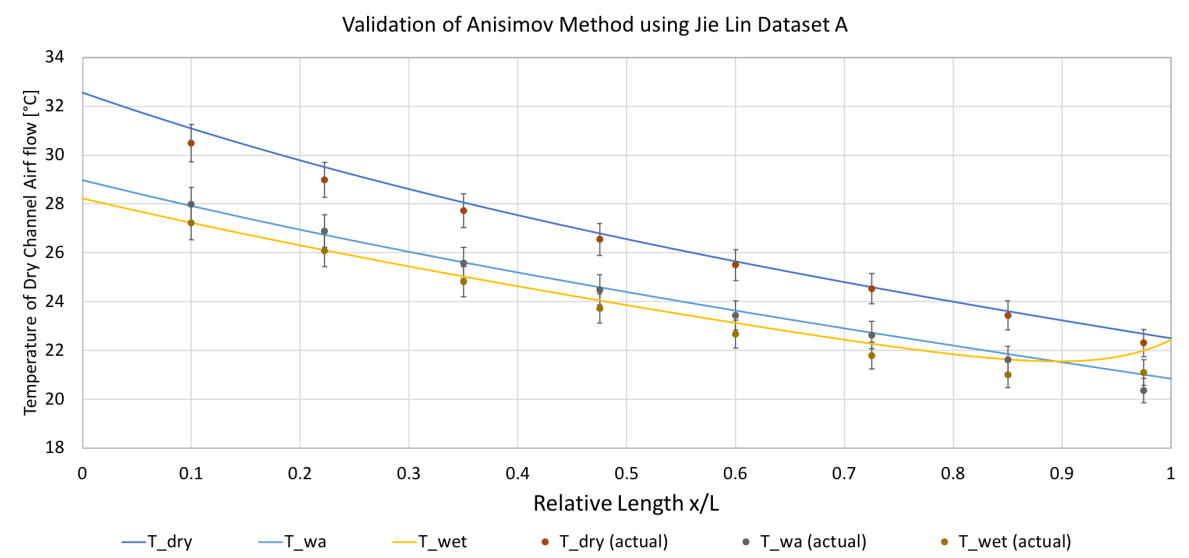

Figure 5b. Simulation for Jie Lin et al.'s dataset A using Anisimov's method (Nu = 4.12). Error bars indicate the range for 2.5% error.

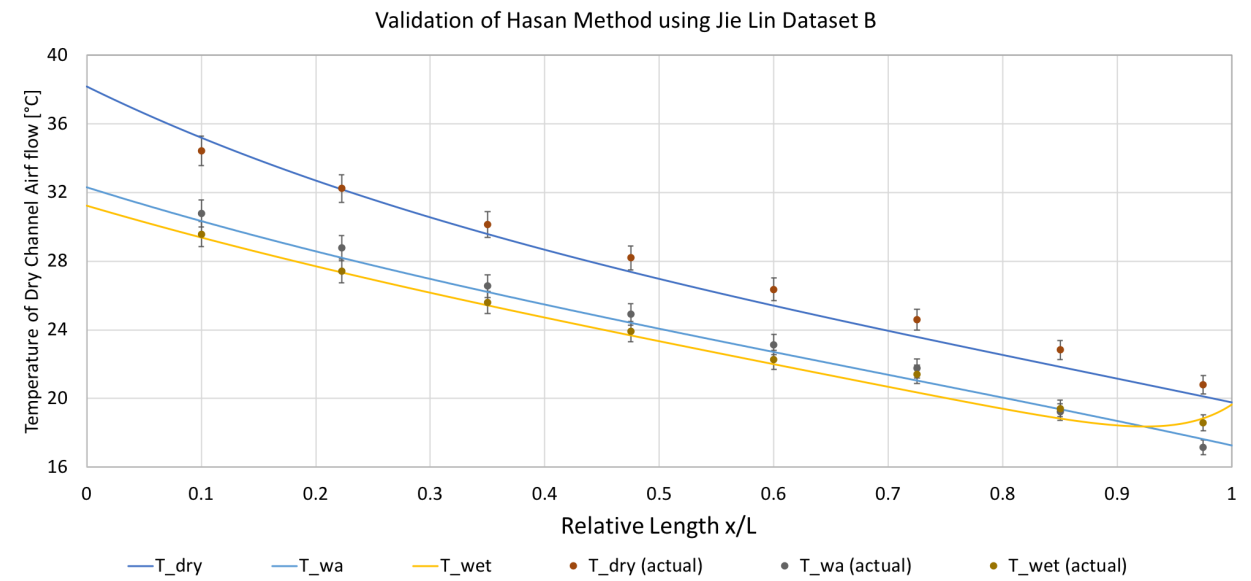

Figure 5c. Simulation for Jie Lin et al.'s dataset B using Hasan's method (Nu = 4.861). Error bars indicate the range for 2.5% error.

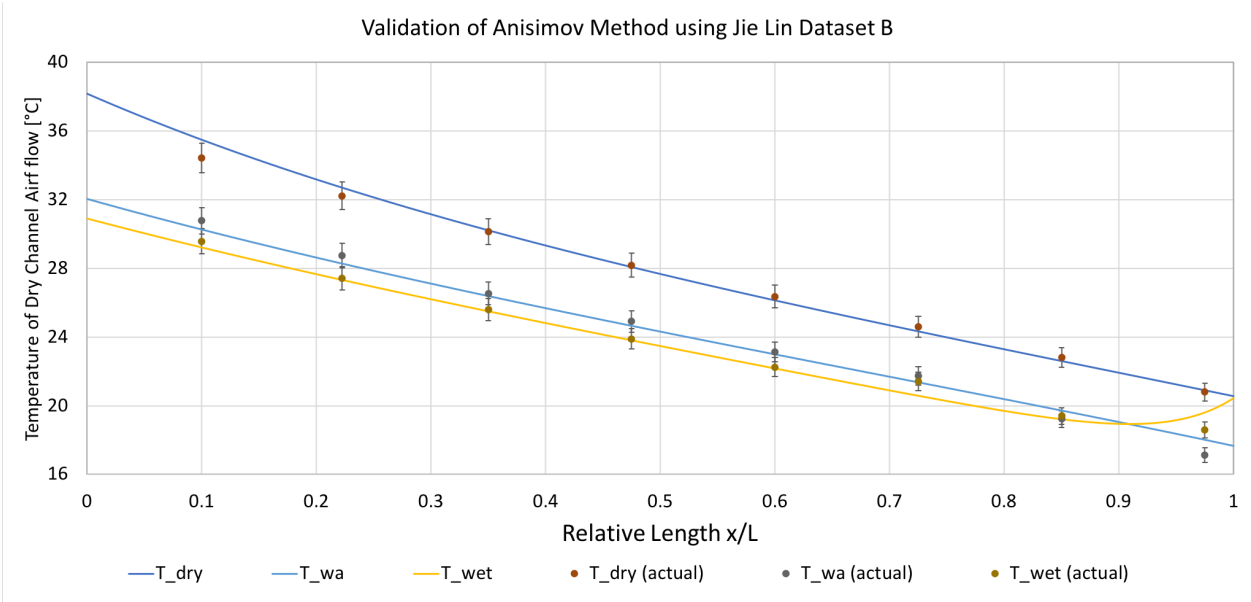

Figure 5d. Simulation for Jie Lin et al.'s dataset B using Anisimov's method (Nu = 4.12). Error bars indicate the range for 2.5% error.

	Hasan's Method (Nu = 4.861)	Anisimov's Method (Nu = 4.12)
Average Error (Dataset A)	0.87 %	1.24 %
Maximum Error (Dataset A)	2.14 %	4.30 %
Average Error (Dataset B)	2.11 %	1.52 %
Maximum Error (Dataset B)	5.03 %	5.60 %

Table 2. Average and maximum errors for each validation trial.

Results & Discussion

In this section, various graphs will be shown with product air temperature on the y-axis and length on the x-axis. Each graph will contain various curves analyzing different parameters such as inlet air temperature, inlet absolute humidity, inlet air velocity, channel height, and working air ratio. There will also be a horizontal line matching the desired output temperature of 24 ^{o}C. By analyzing where the various curves trend below the desired output line, the corresponding channel length can be determined. For all graphs except the one analyzing inlet air temperature, an inlet air temperature of 32 ^{o}C will be used. The constant values and ranges used in each simulation can be found in Table 3.

Parameters	Constant values	Ranges when chosen as free variable
Channel Length [m]	2.0	0.0 - 2.0
Channel Height [mm]	4.0	3.0 - 5.0
Channel Width [m]	0.5	N/A
Inlet Temperature [^{o}C]	32.0	28.0 to 40.0
Inlet Absolute Humidity [g/kg]	13.0	10.0 to 20.0
Inlet Velocity [m/s]	1.0	0.5 to 4.0
Working Air Ratio	0.30	0.2 to 0.5

Table 3. Chosen input conditions for the various simulation trials below. When the specific parameter was not being analyzed, the constant values were chosen, while the ranges were used during each specific analysis.

1. Effect of Inlet Air Temperature

Higher inlet air temperatures predictably have higher outlet air temperatures since a higher inlet temperature would require greater differential temperature differences to decrease to the same outlet temperature. This is evident in Fig. 6 where the inlet temperature of 28 ^{o}C reaches the

comfort level of 24 °C the fastest as well as reaches the lowest temperature after 2 metres. Furthermore, the different temperature curves start to converge as the length is increased. This indicates that successive increases in length are less effective in reducing the overall outlet temperature. Therefore, a shorter IEC around 1 to 1.5 metres in length would be more cost effective. The shortened IEC would be able to cool the room to the desired 24°C except for the most extreme conditions. This would greatly reduce costs as well as reduce the overall size by up to 50%, allowing the IEC to be easier to manufacture and install. An example configuration is shown in Fig. 6 where only an IEC is required to cool a room.

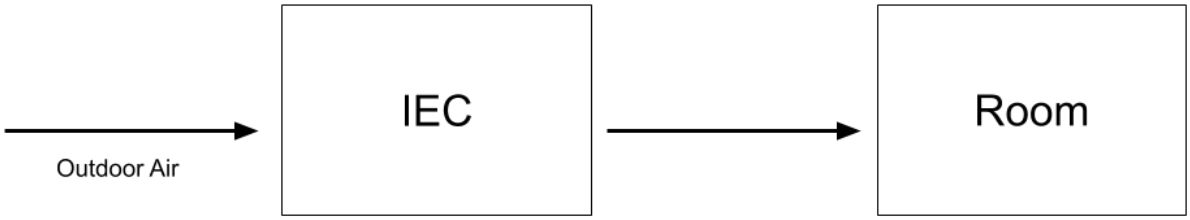

Figure 6. Block diagram showing the basic configuration of an IEC being used to cool a room.

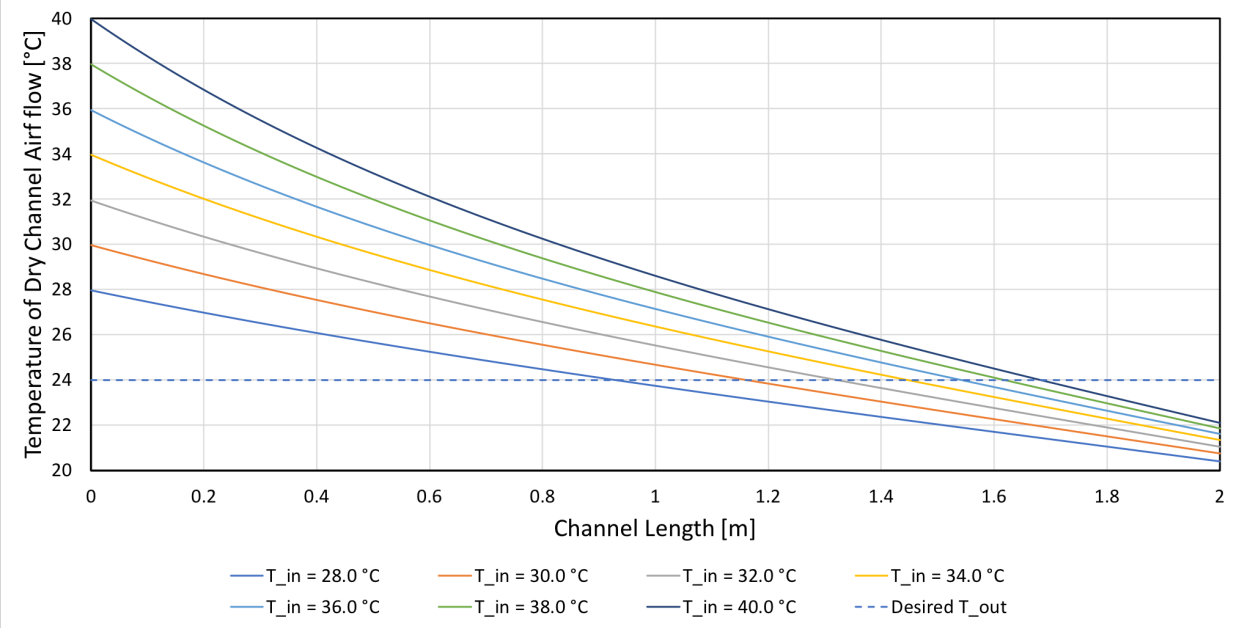

Figure 7. Graph analyzing the effect of varying inlet air temperature between 27.5 °C and 40 °C.

2. Effect of Inlet Absolute Humidity

Changing the inlet absolute humidity ratio also greatly affects the outlet temperature. According to Fig. 8, it is impossible to attain the desired output at inlet humidity ratios above 16 g/kg (given the conditions specified in Table 3). However, an outlet temperature of 24 °C can be achieved by reducing the inlet humidity to 16 g/kg and below. This could be implemented by using the configuration in Fig. 9, where the outdoor air is first passed through a dehumidifier before it is

fed into the IEC. This would not only reduce outlet temperatures, but also shorten the channel length required.

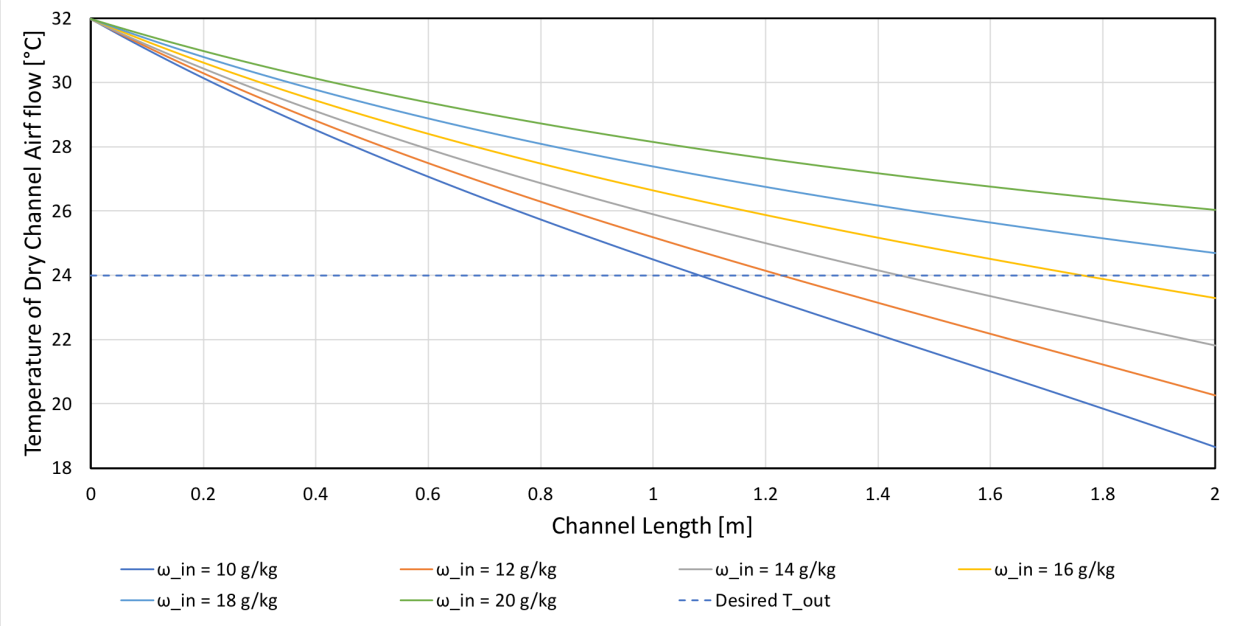

Figure 8. Graph analyzing the effect of varying inlet humidity ratio between 10 g/kg and 20 g/kg.

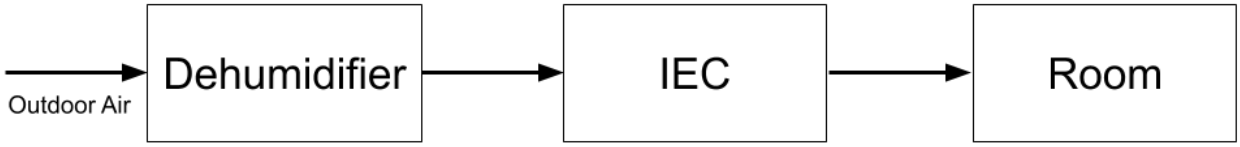

Figure 9. Proposed configuration of a dehumidifier and an IEC in series to effectively cool a room.

3. Effect of Inlet Air Velocity

The graph in Fig. 10 shows that lower inlet air velocities result in a lower outlet temperature. This is because a lower velocity leads to more contact time between the air, the channel plate, and the water film. This allows for more heat to be transferred and thus a lower outlet temperature. Therefore, the intake fan should be set to lower speeds for more effective output. To achieve the desired output temperature of 24 °C, the channel length should be between 1 to 1.5 metres depending on the inlet air velocity. However, if a higher air velocity is required, the desired outlet temperature of 24°C can still be achieved by placing a conventional air conditioning unit immediately after the IEC unit as in Fig. 11. This would still be more efficient than using only a conventional air conditioning unit since the more energy-efficient IEC would first greatly reduce the outlet temperature. For example, rather than cooling hot outdoor air from 32 °C to 24 °C, the IEC could first reduce the temperature to 26 °C and then the conventional unit could cool the remaining 2 °C. In this way, the conventional unit is only used to cool the air by 2 °C rather than 8 °C. This effectively reduces the conventional unit's work required to 25% of the original quantity.

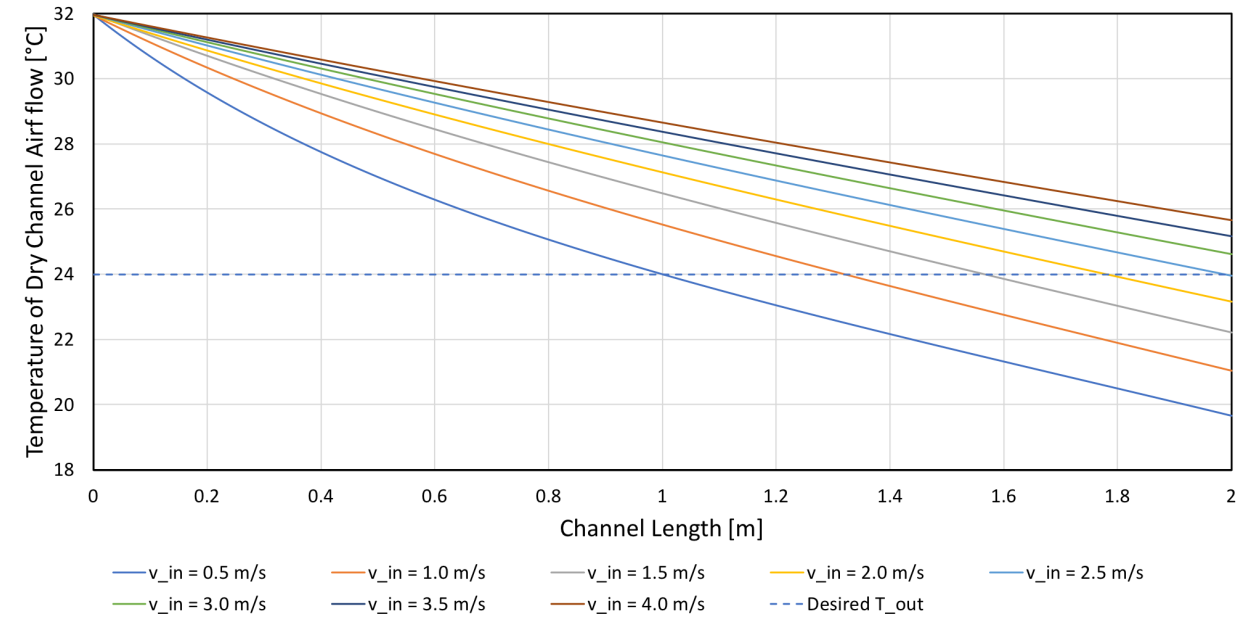

Figure 10. Graph analyzing the effect of varying inlet velocity between 2.0 m/s and 4.0 m/s.

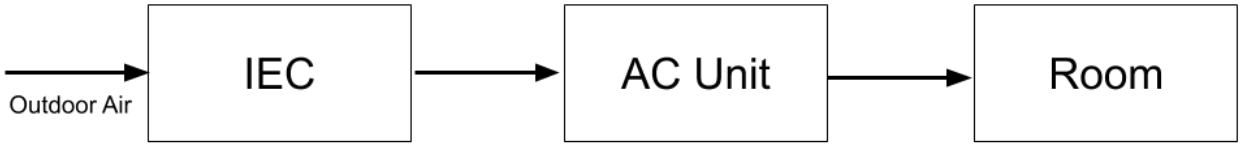

Figure 11. Block diagram showing the proposed configuration of a dehumidifier and an IEC in series to effectively cool a room.

4. Effect of Channel Height

Channel height and the outlet temperature are shown to be directly by the graph in Fig. 12. A smaller channel height causes a smaller hydraulic diameter. This then leads to a greater heat transfer coefficient which corresponds with greater heat transfer values and larger differential temperature changes. As a result, the outlet temperature will be lower for smaller channel heights. Consequently, implementations of IEC units should use smaller channel heights for optimal performance.

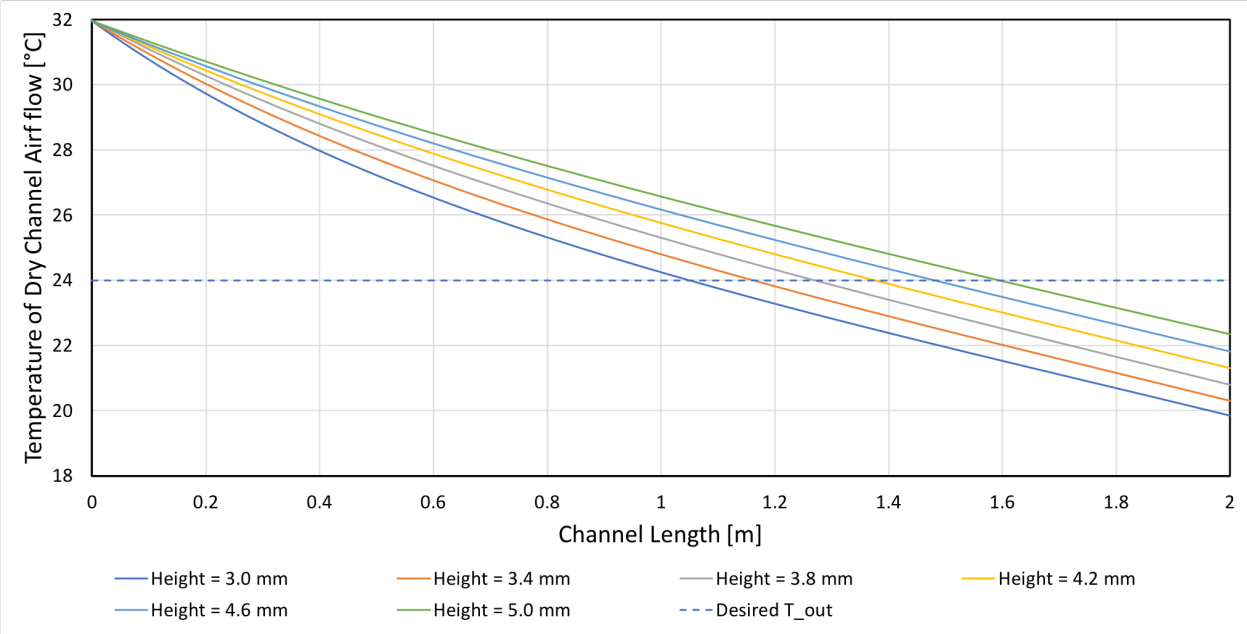

Figure 12. Graph analyzing the effect of varying channel height between 3.0 mm and 5.0 mm.

5. Effect of Working Air Ratio

The graph in Fig. 13 shows that the working air ratio is inversely proportional to the outlet temperature. A larger working air ratio causes a larger mass flow rate in the wet channel. This leads to a smaller differential temperature change in the wet channel, causing a larger temperature gradient to exist. This enables larger sensible heat transfers from the dry channel and larger corresponding differential temperature changes. Thus the temperature will drop more sharply and the outlet temperature will be lower. However, a larger working air ratio greatly reduces the amount of air flow delivered as output. Thus, the working air ratio should only be increased when the resulting decrease in outlet air temperature is significant enough. From Fig. 13, the ideal working air ratio is around 0.3 since the associated temperature curves for the higher ratios are relatively bunched up. This means that an increase in working air ratio would have less impact on the outlet air temperature. Finally, a working air ratio still allows a channel length under 1.2 metres to be used.

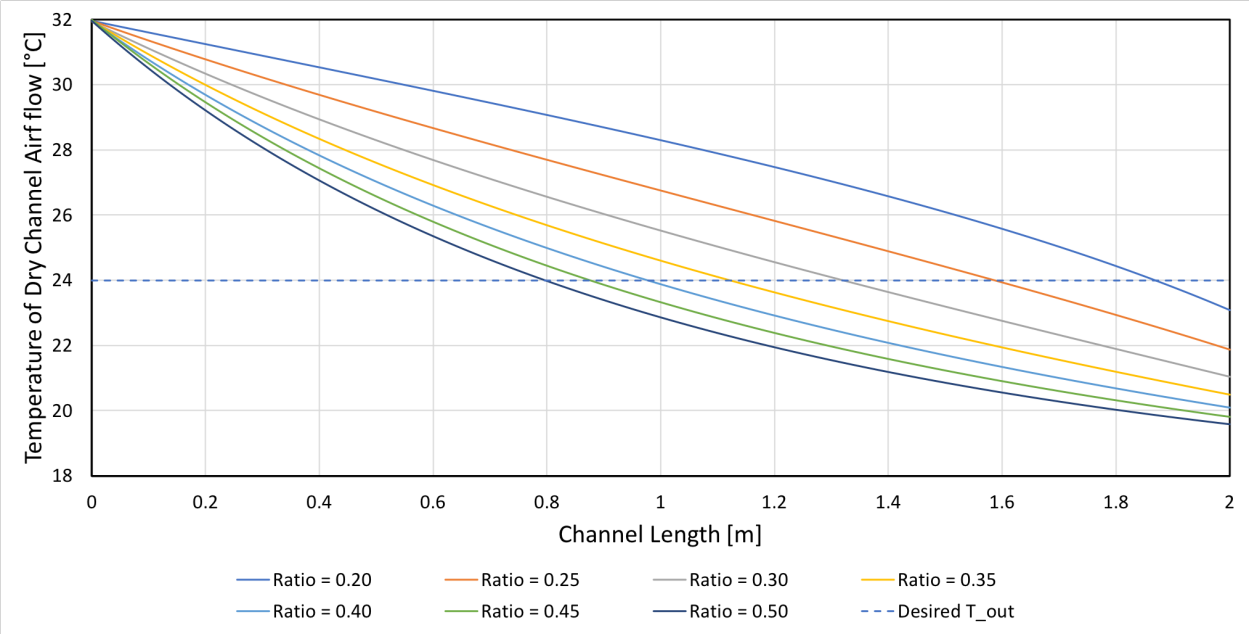

Figure 13. Graph analyzing the effect of varying inlet humidity ratio between 0.20 and 0.50.

Conclusion

In this paper, a working 1D simulation method was developed that effectively produced results matching known experimental results. Through validation against existing experimental results in literature, the model was found to have a maximum error of 5.60 % and an average error below 2 %. Furthermore, various design configurations were explored to find the most appropriate setup given certain input conditions and desired outputs. Using the mathematical model and simulation method, it was determined that the ideal IEC design used a channel length of around 1 to 1.5 metres and a working air ratio around 0.3.

References

[1] Meteorological Service Singapore, “Climate of Singapore,” *Climate of Singapore*. [Online]. Available: http://www.weather.gov.sg/climate-climate-of-singapore/. [Accessed: 25-Jul-2019].
[2] A. Bouchama and J. P. Knochel, “Heat Stroke,” *New England Journal of Medicine*, vol. 346, no. 25, pp. 1978–1988, 2002.
[3] I. Sarbu, “A review on substitution strategy of non-ecological refrigerants from vapour compression-based refrigeration, air-conditioning and heat pump systems,” *International Journal of Refrigeration*, vol. 46, pp. 123–141, 2014.
[4] K. Chua, S. Chou, W. Yang, and J. Yan, “Achieving better energy-efficient air conditioning – A review of technologies and strategies,” *Applied Energy*, vol. 104, pp. 87–104, 2013.
[5] A. Hasan, “Going below the wet-bulb temperature by indirect evaporative cooling: Analysis using a modified ε-NTU method,” *Applied Energy*, vol. 89, no. 1, pp. 237–245, 2012.

[6] C. Zhan, Z. Duan, X. Zhao, S. Smith, H. Jin, and S. Riffat, “Comparative study of the performance of the M-cycle counter-flow and cross-flow heat exchangers for indirect evaporative cooling – Paving the path toward sustainable cooling of buildings,” *Energy*, vol. 36, no. 12, pp. 6790–6805, 2011.
[7] B. Riangvilaikul and S. Kumar, “An experimental study of a novel dew point evaporative cooling system,” *Energy and Buildings*, vol. 42, no. 5, pp. 637–644, 2010.
[8] S. Anisimov, D. Pandelidis, A. Jedlikowski, and V. Polushkin, “Performance investigation of a M (Maisotsenko)-cycle cross-flow heat exchanger used for indirect evaporative cooling,” *Energy*, vol. 76, pp. 593–606, 2014.
[9] M. H. Mahmood, M. Sultan, T. Miyazaki, S. Koyama, and V. S. Maisotsenko, “Overview of the Maisotsenko cycle – A way towards dew point evaporative cooling,” *Renewable and Sustainable Energy Reviews*, vol. 66, pp. 537–555, 2016.
[10] D. Pandelidis, A. Cichoń, A. Pacak, S. Anisimov, and P. Drąg, “Counter-flow indirect evaporative cooler for heat recovery in the temperate climate,” *Energy*, vol. 165, pp. 877–894, 2018.
[11] R. Chengqin and Y. Hongxing, “An analytical model for the heat and mass transfer processes in indirect evaporative cooling with parallel/counter flow configurations,” *International Journal of Heat and Mass Transfer*, vol. 49, no. 3-4, pp. 617–627, 2006.
[12] X. Cui, K. Chua, M. Islam, and W. Yang, “Fundamental formulation of a modified LMTD method to study indirect evaporative heat exchangers,” *Energy Conversion and Management*, vol. 88, pp. 372–381, 2014.
[13] D. Pandelidis, A. Cichoń, A. Pacak, S. Anisimov, and P. Drąg, “Performance comparison between counter- and cross-flow indirect evaporative coolers for heat recovery in air conditioning systems in the presence of condensation in the product air channels,” *International Journal of Heat and Mass Transfer*, vol. 130, pp. 757–777, 2019.
[14] A. Hasan, “Indirect evaporative cooling of air to a sub-wet bulb temperature,” *Applied Thermal Engineering*, vol. 30, no. 16, pp. 2460–2468, 2010.
[15] S. Anisimov, D. Pandelidis, and J. Danielewicz, “Numerical study and optimization of the combined indirect evaporative air cooler for air-conditioning systems,” *Energy*, vol. 80, pp. 452–464, 2015.
[16] C. Zhan, X. Zhao, S. Smith, and S. Riffat, “Numerical study of a M-cycle cross-flow heat exchanger for indirect evaporative cooling,” *Building and Environment*, vol. 46, no. 3, pp. 657–668, 2011.
[17] S. Anisimov and D. Pandelidis, “Numerical study of the Maisotsenko cycle heat and mass exchanger,” *International Journal of Heat and Mass Transfer*, vol. 75, pp. 75–96, 2014.
[18] S. Anisimov and D. Pandelidis, “Theoretical study of the basic cycles for indirect evaporative air cooling,” *International Journal of Heat and Mass Transfer*, vol. 84, pp. 974–989, 2015.
[19] Rogers G.F.C. and Mayhew Y. R, Thermodynamic and Transport Properties of Fluids, 5th ed., Blackwell, Oxford, U.K. 1998
[20] J. Lin, D. T. Bui, R. Wang, and K. J. Chua, “On the fundamental heat and mass transfer analysis of the counter-flow dew point evaporative cooler,” *Applied Energy*, vol. 217, pp. 126–142, 2018.